

Rapid and sheet-to-sheet slot-die coating manufacture of highly efficient perovskite solar cells processed under ambient air

Yu-Ching Huang^{a,*}, Chia-Feng Li^a, Zhi-Hao Huang^a, Po-Hung Liu^a, Cheng-Si Tsao^{b,c,*}

^a Department of Materials Engineering, Ming Chi University of Technology, New Taipei City 24301, Taiwan

^b Institute of Nuclear Energy Research, Taoyuan 32546, Taiwan

^c Department of Materials Science and Engineering, National Taiwan University, Taipei 10617, Taiwan

ARTICLE INFO

Keywords:

Perovskite solar cell
Near-infrared radiation
Two-steps
GIWAXS
GISAXS
Slot-die

ABSTRACT

A nitrogen-free and slot-die coating fabrication of perovskite solar cells combined with NIR annealing. We develop a fabrication approach of planar inverted structured perovskite solar cell (PSC) in ambient condition with a PCE of 12.4% as compared to that (13.3%) of PSC fabricated in glove box filled with nitrogen. In addition, we demonstrate an alternative post-annealed method by near-infrared (NIR) radiation to traditional heating method by oven. The annealed time by NIR can be shortened from 1500 s to 30 s and the device performance over 10% can be achieved. The present work investigates the NIR effect for different layers in the two-step processing on the cell performance. The grazing-incidence wide-angle and small-angle X-ray scattering (GIWAXS and GISAXS) techniques for the perovskite layers are performed to reveal the crystalline and nano-morphological structures of perovskite layers correlated to thermal and NIR annealing effects. Based on this approach under ambient air, we scale up to the large-area fabrication using the slot-die coating. The performance of slot-die coated PSC can achieve to 12.3%. The critical step is the control of PbI_2 layer thickness. We also applied the NIR radiation to the slot-die coated PSC and the PCE of 11.4% can be achieved. Our study paves a facile way to rapid manufacture and mass production of perovskite solar cells.

1. Introduction

Organometal trihalide perovskite photovoltaic devices have recently drawn lots of attentions due to the properties of high absorption coefficient, broad absorption range, outstanding charge carriers mobility and long diffusion length (Stranks et al., 2013; Yu et al., 2017; De Wolf et al., 2014; Kagan et al., 1999). The power conversion efficiency (PCE) of the perovskite solar cells (PSCs) has significantly increased from 3.1% to 22.1% in these years (Yang et al., 2017). The hybrid perovskite photovoltaics were initially fabricated based on the device structure of the solid dye sensitized solar cells (DSSCs) (Kojima et al., 2009). Device performance by using DSSCs structure achieved several milestones (Yang et al., 2015; Jeon et al., 2015). These devices have the mesoporous TiO_2 scaffold to support the perovskite materials. However, the mesoporous devices need a high temperature sintering that could increase the processing time and cost of mass-production. Recently, a simple and low cost planar heterojunction structure of perovskite solar cell has been developed without using mesoporous TiO_2 scaffold. The first successful planar heterojunction structure can be traced back to the

perovskite/fullerene structure reported by Guo, showing a PCE of 3.9% (Jeng et al., 2013). Recently, the PCE of the planar structure was pushed over 19% through perovskite film morphology control and interface engineering (Zhou et al., 2014). These results showed that the planar heterojunction structure can achieve similar device performance as the mesoporous structure. The planar structure can be divided into regular (n-i-p) and inverted (p-i-n) structure depending on which selective contact is used on the bottom. The p-i-n structure is derived from the organic solar cell. Several charge transport layers usually used in organic solar cells were successfully transferred into perovskite solar cells (You et al., 2014). The poly(3,4-ethylenedioxythiophene):poly(styrenesulfonate) (PEDOT:PSS) and fullerene derivative were directly implemented as the hole transport layer (HTL) and electron transport layer (ETL) in the perovskite solar cells. Due to the choice of these materials, the inverted-structured perovskite devices showed the advantages of high efficiency, lower temperature processing and flexibility (You et al., 2014). For the frequently-used one-step preparation of perovskite materials, a solution containing $\text{CH}_3\text{NH}_3\text{I}$ and lead halide salt (PbCl_2 , PbI_2 and PbBr_2) dissolved in N,N-dimethylformamide

* Corresponding authors at: Ming Chi University of Technology, New Taipei City 24301, Taiwan (Y.-C. Huang). Institute of Nuclear Energy Research, Taoyuan 32546, Taiwan (C.-S. Tsao).

E-mail addresses: huangyc@mail.mcut.edu.tw (Y.-C. Huang), cstsoa@iner.gov.tw (C.-S. Tsao).

<https://doi.org/10.1016/j.solener.2018.11.020>

Received 18 May 2018; Received in revised form 15 October 2018; Accepted 6 November 2018

Available online 15 November 2018

0038-092X/ © 2018 Elsevier Ltd. All rights reserved.

(DMF) is deposited onto the substrate. The deposited perovskite precursor layer was heated at the temperature over 100 °C for 10 ~ 60 min to evaporate residual solvent from the film and also to control the crystallisation of the perovskite layer. The long heating time for the perovskite layer is a bottleneck to the mass-production or rapid manufacturing of perovskite solar cells. Moreover, the PCE of the perovskite solar cells is not stable after the devices are fabricated under ambient atmosphere due to the commercial requirements, such as low-cost and easy fabrication.

Perovskite films is the core of the performance of perovskite solar cells. The fabrication of the perovskite films can be divided into two kinds, one-step and two-step deposition approaches. Although the one-step deposition has been broadly used due to the simple process, the naturally crystallized perovskite film often exhibited an anisotropic growth, leading to low uniformity and poor coverage (Dualeh et al., 2014; Yantara et al., 2015). This low uniformity limited the perovskite solar cells to be applied to large-area mass-production. For the two-step deposition, PbI_2 layers are firstly deposited on the substrate via various approaches to obtain the PbI_2 layers with good uniformity and coverage. Hence, we think the two-step deposition is more suitable for mass-production process at the current status.

Due to the fast progress in PCE of perovskite solar cells, there have been a few investigations into the field of large-area PSC manufacture, such as doctor blading (Deng et al., 2015), spray coated (Das et al., 2015; Huang et al., 2016) and slot-die coating (Hwang et al., 2015; Cotella et al., 2017; Zuo et al., 2018; Kim et al., 2018). Among these approaches, slot-die coating process is deemed as a high throughput process with low materials waste, and is also a proven technique suitable for roll-to-roll process. Roll-to-roll compatible process for manufacturing PSCs has been proposed in recent years (Hwang et al., 2015; Cotella et al., 2017; Zuo et al., 2018; Kim et al., 2018; Qin et al., 2017; Ciro et al., 2017; Di Giacomo et al., 2018). The vacuum-free slot-die coated process was developed by using “gas-quenching” approach (Hwang et al., 2015; Qin et al., 2017), which is attached an additional slot-die head for high-pressure N_2 gas to quickly dry the PbI_2 film. This approach presents a facile way to form a good perovskite film by slot-die coating, however, the device area is only about 0.1 cm^2 implies that it is not easy to manufacture a large-area film with high uniformity by controlling the N_2 gas. The large-area PSCs module (> 150 cm^2) was performed in recent literature and the PCE of ~12% can be achieved (Di Giacomo et al., 2018). This study demonstrates a great potential for the commercialization of PSCs, but the slot-die process was performed in the glove-box. Previous studies demonstrated that the additional humidity buffer or inert gas flow are needed for the perovskite fabrication due to the moisture sensitivity of perovskite films (Yang et al., 2017; Peiris et al., 2017; Zeng et al., 2017). For the two-step slot-die coating PSCs, the PCE of 14.7% can be achieved (Qin et al., 2017). However, these studies usually need longer annealing times (> 10 min) to form uniform and dense perovskite films. This is still a limitation for the rapid mass-production process. Recently, some rapid light-based annealing strategies have been demonstrated for the efficient PSC fabrication. For instance, near-infrared annealing of a PSC based on the Al_2O_3 scaffold for 2.5 s achieved a PCE of 10.0% (Troughton et al., 2015). Other study utilized flash photonic annealing to heat perovskite films for 1.15 ms, and achieved the PCE of 11.3% (Troughton et al., 2016). However, these studies used the lab-scale spin coating process to fabricate the PSC, and mainly focus on the high-temperature-processed TiO_2 to obtain good device performance.

Slot-die coating technique is proven to be a high throughput and low-cost process for the mass-production of PSCs. However, developing a rapid and facile way to fabricate large-area PSCs under ambient condition is still needed. In our previous studies, we have successfully applied the slot-die coating technique for printing large-area organic photovoltaics and modules (Huang et al., 2017, 2016). Therefore, we further employed the slot-die coating process in the fabrication of PSCs. For solving the mentioned problems toward commercialization of

perovskite solar cell, we present an alternative method for annealing perovskite film which reduces the conventionally long annealing time to as less than 30 s whilst maintaining the PCE. This method adopted the commercially available near-infrared (NIR) radiation to rapidly cure the perovskite film. We also successfully developed a fabrication method of perovskite solar cell under ambient atmosphere (i.e., humid air of ~R.H. 60% or more), which was based on the two-step processing. For fundamentally understanding, the synchrotron grazing-incidence wide-angle and small-angle X-ray scattering technique (GI-WAXS/GISAXS) techniques were performed to investigate the hierarchical structure of perovskite crystalline films annealed by NIR and oven. The relationship between performance and structure are revealed. Finally, we combined the developed techniques with large-area fabrication of slot-die coating. The PbI_2 layer thickness (concentration) in the two-step slot-die coating plays an important role for achieving high performance. The satisfying result would demonstrate this useful approach for the mass-production or commercialization of perovskite solar cells. Our work is the first study combining NIR annealing and the manufacture of slot-die coating PSCs based on low-temperature p-i-n structure. Our study not only provides the insight into the rapid annealing process of the low-temperature processed PSCs but also paves another facile way for the PSCs commercialization.

2. Experimental

For fabricating perovskite device as reference, the ITO-coated glass was successively ultrasonic cleaned for 30 min in deionized water, acetone and isopropanol, respectively. These substrates were then treated with nitrogen plasma cleaning for 10 min. The PEDOT:PSS HTL was spin-coated on the ITO-coated substrate at 5000 rpm for 30 s and was then annealed at 130 °C for 10 min. For deposited the perovskite active layer, a PbI_2 precursor solution (1 M, 461 mg/ml) in DMF was prepared by stirring at 70 °C for 2 hr under ambient air. The solution was cooled to room temperature and then transferred to the glove box and finally spin-coated on the PEDOT:PSS layer at 6000 rpm for 10 s. The PbI_2 film was then heated at 70 °C for 10 min. The $\text{CH}_3\text{NH}_3\text{I}$ (MAI) solution of 50 mg/ml solution in IPA was prepared for perovskite conversion. We spin-coated the MAI solution on the PbI_2 film and the film color would change to a dark brown immediately due to the perovskite conversion. It is so-called two-step processing. The reference device is prepared under the nitrogen environment. For considering the atmosphere effect for each, the PbI_2 layer or perovskite layer converted by MAI solution was spin-coated, respectively, under ambient atmosphere (/or air with ~R.H. 60%) condition in which the other step in two-step process is treated under nitrogen. The perovskite films were annealed at the 100 °C for 15 min. On the other hand, the PbI_2 and perovskite layers were annealed by the NIR for developing the rapid manufacture technique to replace the thermal annealing. The NIR equipment (MNIR 2525, MOS Technology Inc., Taiwan) exhibits an output spectrum in the region of 380–2500 nm and the peak value is 800 nm \pm 100 nm. The maximum power density of the NIR equipment is 200 kW/m^2 , and the NIR output power density was controlled by varying the lamp power and the exposure duration. The distance between the lamps and samples was kept at 10 cm, and the radiation exposure time was controlled by varying the moving speed of a conveyor system beneath the lamp. After the perovskite film formation, we spin-coated the (Kojima et al., 2009, 2009)-phenyl-C61-butyric acid methyl ester (PCBM) layer and polyethylenimine (PEI) as the ETL and buffer layer, respectively, on the perovskite film. At last, the devices were carried to a vacuum evaporator and were deposited 100 nm of Ag as the metal electrode. The schematic of the devices are shown in Fig. 1. In addition, we slot-die coated the PbI_2 layer by using Coatema coating system (Coatema, easycoater, Germany). The slot-die coating speed and input rate used for PbI_2 layer were 1 m/min and 0.5 ml/min, respectively. Moreover, we also tuned the concentration of PbI_2 from 1 M to 0.5 M to obtain the optimal thickness of slot-die coated film. All devices used in this study

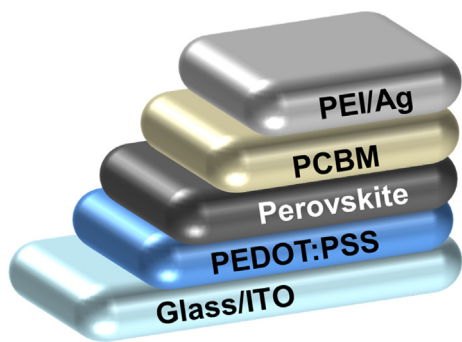


Fig. 1. Schematic of perovskite solar cells.

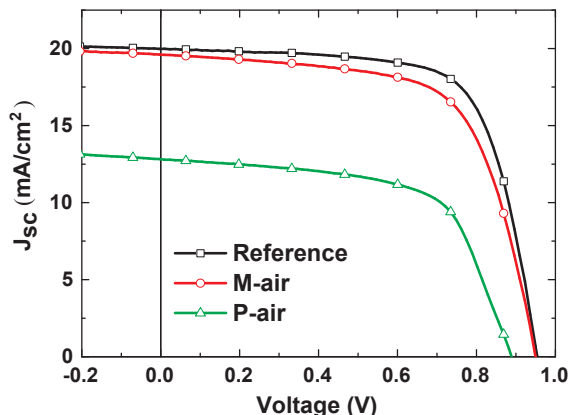


Fig. 2. J-V curves of perovskite solar cells based on PbI₂ and perovskite layers formed under different conditions.

were with the area of $1 \times 0.3 \text{ cm}^2$, and the performance of the devices were characterized by a solar simulator under AM 1.5G, 100 mW/cm^2 irradiation. The simultaneous GISAXS/GIWAXS measurements were performed at BL-23A beam line of National Synchrotron Radiation Center, Taiwan (Huang et al., 2015). The scattering intensities were reduced through the standard calibration and background subtraction and are expressed as a function of scattering vector, Q , where $Q = 4\pi(\sin \theta)/\lambda$, θ is half of the total scattering angle, and λ is the X-ray wavelength.

3. Results and discussion

In order to facilitate the manufacture the PSCs under atmosphere (/or humid air) condition, we firstly investigated the effect of atmosphere for different layers on the performance of PSCs. For the reference device, we spin coated the perovskite film via the mentioned two-step processing in a glove box filled with nitrogen. For PSCs fabricated with the atmosphere effect mentioned, we named the PSC with PbI₂ layer (the first step) coated under air and the perovskite formation (the second step) under nitrogen as P-air. The PSC with PbI₂ layer coated under nitrogen and the perovskite formation under air named as M-air. The current-voltage (J-V) characteristics of these devices are shown in

Table 1

Performance of perovskite solar cells corresponding to Fig. 2. Values are for the highest-PCE device, and the average data are obtained from 5 devices in the brackets.

Samples	J_{sc} (mA/cm ²)	V_{oc} (V)	FF (%)	PCE (%)
Reference	19.98 (18.96 ± 0.74)	0.95 (0.95 ± 0)	69.8 (71.53 ± 1.43)	13.3 (12.9 ± 0.29)
M-air	19.62 (18.73 ± 1.03)	0.95 (0.94 ± 0.01)	65.2 (67.03 ± 1.55)	12.2 (11.83 ± 0.39)
P-air	12.83 (13.91 ± 0.9)	0.89 (0.89 ± 0.03)	62.6 (55.73 ± 5.3)	7.1 (6.83 ± 0.38)

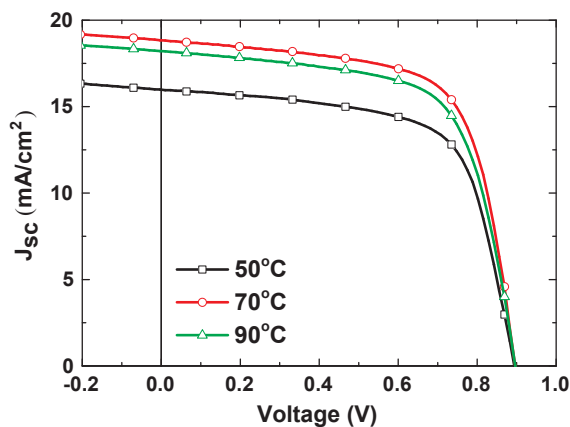


Fig. 3. J-V curves of perovskite solar cells based on PbI₂ layer deposited on substrates with different temperatures.

Table 2

Performance of perovskite solar cells based on PbI₂ layer deposited on substrates with different temperatures. Values are for the highest-PCE device, and the average data are obtained from 5 devices in the brackets.

Heat Temp. (°C)	J_{sc} (mA/cm ²)	V_{oc} (V)	FF (%)	PCE (%)
50	15.99 (15.66 ± 0.52)	0.89 (0.92 ± 0.02)	66.2 (63.83 ± 2.25)	9.5 (9.17 ± 0.25)
70	18.84 (18.12 ± 0.55)	0.90 (0.9 ± 0.01)	67.4 (70.07 ± 2.55)	11.4 (11.37 ± 0.05)
90	18.29 (17.39 ± 0.67)	0.90 (0.92 ± 0.01)	65.9 (66.5 ± 1.45)	10.8 (10.63 ± 0.12)

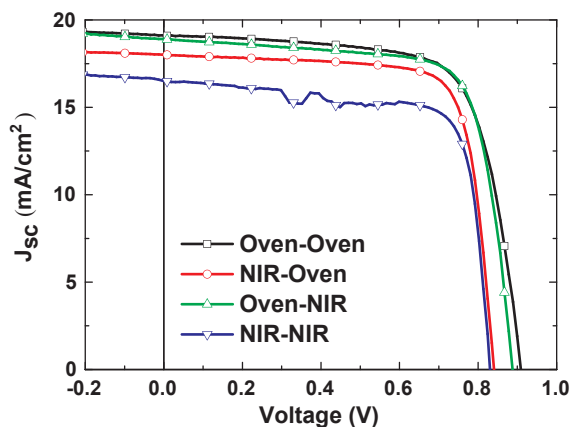


Fig. 4. J-V curves of perovskite solar cells based on the two-step annealed by the combination of oven and NIR.

Fig. 2 and listed in Table 1. The reference device fully coated in N₂ exhibit a PCE of 13.3%, but the P-air device shows a low PCE of 7.1% due to the dramatically decrease of short-circuit current (J_{sc}) and fill

Table 3

Performances of perovskite solar cells based on the two-step annealed by the combination of oven and NIR. Values are for the highest-PCE device, and the average data are obtained from 5 devices in the brackets.

Heat method	J_{sc} (mA/cm ²)	V_{oc} (V)	FF (%)	PCE (%)
Oven-Oven	19.12 (18.82 ± 0.37)	0.91 (0.91 ± 0)	71.1 (71 ± 0.37)	12.4 (12.17 ± 0.21)
NIR-Oven	18.01 (18.01 ± 0.41)	0.84 (0.85 ± 0.01)	77 (74.23 ± 1.96)	11.7 (11.37 ± 0.4)
Oven-NIR	18.91 (18.34 ± 0.41)	0.89 (0.88 ± 0.01)	74.1 (75.57 ± 1.07)	12.4 (12.23 ± 0.17)
NIR-NIR	16.52 (16.95 ± 0.31)	0.83 (0.85 ± 0.01)	75.7 (72.2 ± 2.5)	10.4 (10.37 ± 0.05)

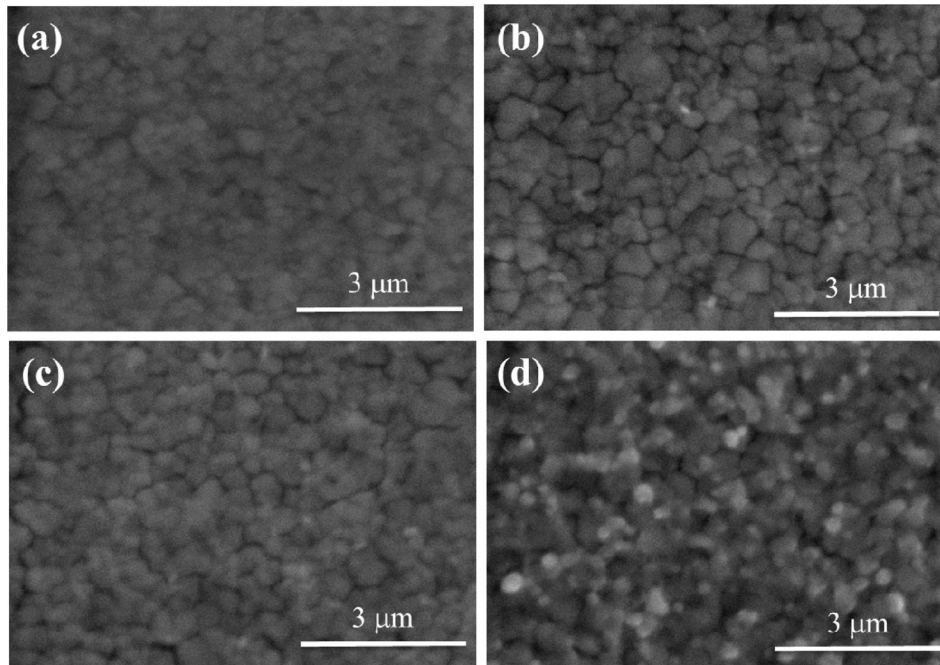


Fig. 5. Top-view SEM images of the perovskite layers annealed by the combination of oven and NIR. (a) Oven-Oven, (b) NIR-Oven, (c) Oven-NIR and (d) NIR-NIR.

factor (FF). However, the M-air device shows a similar PCE of 12.2% to the reference devices. This result implies that the PbI_2 layer is sensitive to the air (including oxygen and humidity, R.H. 50 ~ 60%, here). The perovskite layer via MAI deposition can be formed under atmosphere condition with slight reduction in PCE. Therefore, how to control the PbI_2 formation under humid air is a critical step for the successful fabrication of perovskite solar cells under atmosphere condition.

In order to solve the problem of fabricating the perovskite solar cells in ambient atmosphere (or humid air), we try to heat the ITO-coated substrate at various temperatures and then deposit the PbI_2 film on the warm substrate. The related J-V curves and photovoltaic characteristics are shown and listed in Fig. 3 and Table 2, respectively. From these results, we can observe that increasing substrate temperature can enhance the performance of PSCs due to the improvement of PbI_2 film formation. The high substrate temperature would shorten the PbI_2 film formation time so that the PbI_2 film is impacted less by the oxygen and humidity. As compared to the non-heated substrate, the J_{sc} increases from 12.83 to 15.99 mA/cm² as the substrate is at 50 °C. The J_{sc} slightly decreases with increasing substrate temperature to 70 °C and 90 °C. The optimal J_{sc} achieved 18.84 mA/cm² at the substrate temperature of 70 °C. Meanwhile, the FF was also improved to 67.4% and the resulting PCE achieved 11.4%. This PCE is almost comparable to the previous PCE of M-air device (PbI_2 is coated herein under nitrogen). According to our results, we provide a facile way to well-control the quality of PbI_2 crystalline layer under humid air and obtain a good PCE of devices fully manufactured under ambient atmosphere condition. It can be also

concluded that appropriately heating the PbI_2 layer or shortening the time of PbI_2 crystallization is a necessary step for the fabrication under the ambient air.

To largely shorten the post thermal-annealing time of the perovskite films, we use the alternative heating system of NIR radiation to conventional oven. Based on what we propose for two-step processing under humid air, we need to anneal the PbI_2 layer and perovskite layer converted by MAI solution separately. For preparing the reference device, the PbI_2 layer and perovskite layer are treated at 70 °C for 600 s and 100 °C for 900 s in the oven, respectively. We named this reference device as “oven-oven”. On the other hand, we used NIR to anneal either PbI_2 layer (the first step) or perovskite layer (the second step) with the other step was annealed in the oven. The device based on PbI_2 layer annealed by NIR and perovskite layer annealed by the oven is named as “NIR-Oven”. Similarly, the device based on PbI_2 layer annealed by the oven and perovskite layer annealed by NIR is named as “Oven-NIR”. The device based on both PbI_2 and perovskite layers annealed by NIR is named as “NIR-NIR”. A roughly optimum annealing time by NIR is 15 s. The related J-V curves and performance of PSCs are shown in Fig. 4 and listed in Table 3, respectively. The PCE of the reference device is 12.4%. The reference device exhibits a J_{sc} of 19.12 mA/cm², V_{oc} of 0.91 V and FF of 71.1%, showing the good J_{sc} and FF. For the NIR-Oven device, the PCE would be reduced to 11.7%. The reduction in PCE mainly resulted from the decrease of V_{oc} and J_{sc} . However, the Oven-NIR device remains a similar PCE to the Oven-Oven device. These results confirm that the PbI_2 layer is more sensitive to the NIR process than perovskite

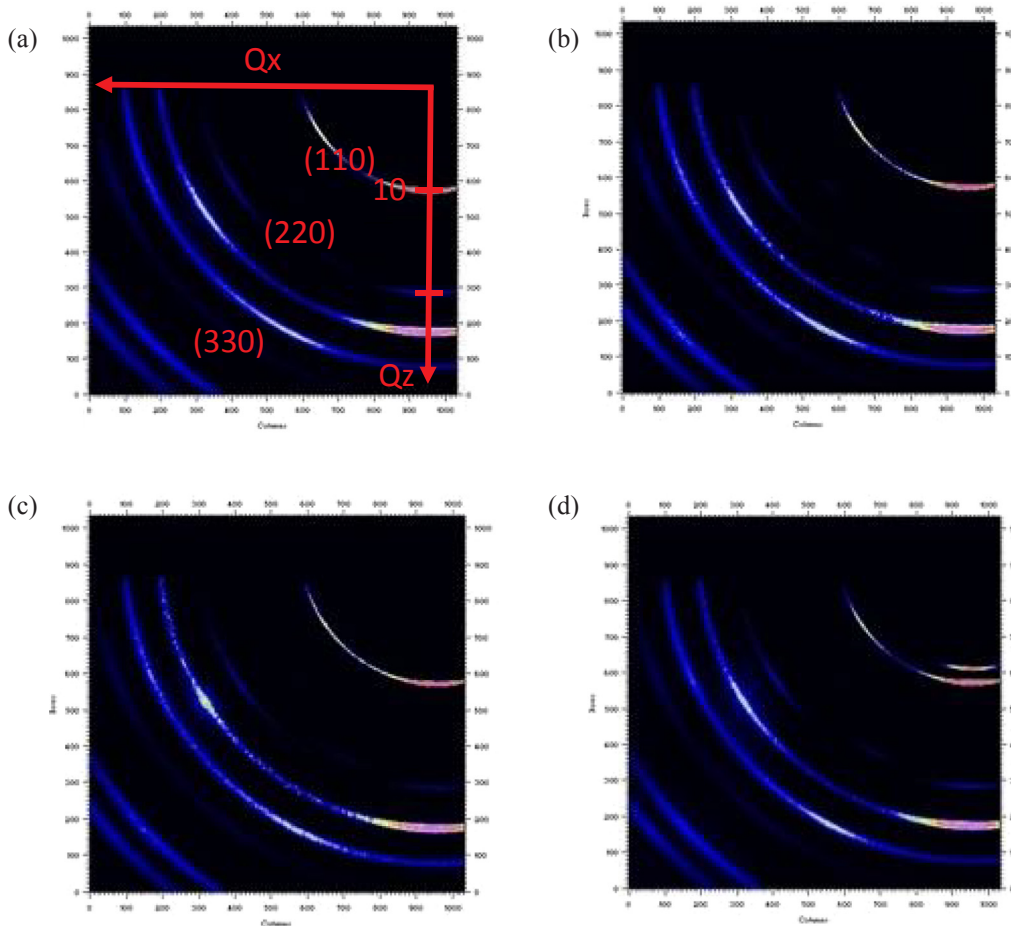


Fig. 6. Two dimensional GIWAXS patterns of the perovskite layers annealed by the combination of oven and NIR. (a) Oven-Oven, (b) NIR-Oven, (c) Oven-NIR and (d) NIR-NIR.

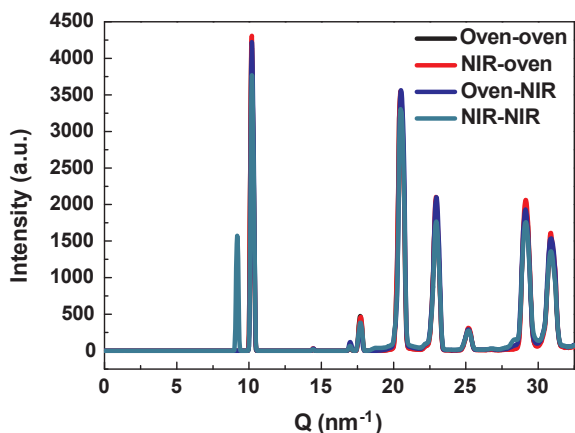


Fig. 7. Ring-averaged GIWAXS profiles corresponding to Fig. 5.

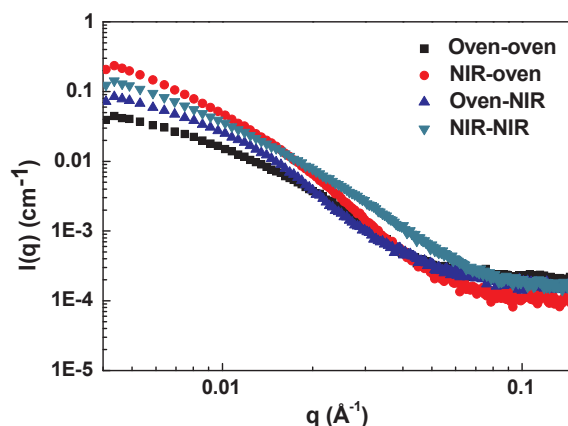


Fig. 8. GISAXS profiles of the perovskite layers annealed with the conditions corresponding to Table 3.

layer. Finally, we anneal both PbI_2 layer and perovskite layer by NIR, resulting in PCE of 10.5%. Although the PCE of device fully post-annealed by NIR has the loss of $\sim 16\%$ compared to the device fully post-annealed by oven, the processing time can be shortened from 1500 s to 30 s. NIR irradiation instead of thermal annealing shows its potential for the quick mass-production. We think that the performance of PSCs could be further enhanced by optimizing more irradiation parameters of the NIR annealing process.

From the fundamental or mechanistic viewpoint, the present study needs to investigate (1) what is the difference between the inner films

annealed by thermal oven and NIR technique, and (2) how is the reduction in device performance correlated with the film structure annealed by NIR? First of all, we characterized the morphology of ITO/PEDOT:PSS/perovskite films varying with annealing approaches by scanning electron microscope (SEM) (Fig. 5). In addition, the PbI_2 layers annealing by oven and NIR are shown in supporting information (Fig. S1). For the Oven-Oven devices, we observe the perovskite films with grain sizes of ~ 300 nm. In Fig. 6(b) and (c), these films exhibit a slightly uneven distribution of grains due to the fast process. However, the good coverage of these films is still performed, only a few pin-holes

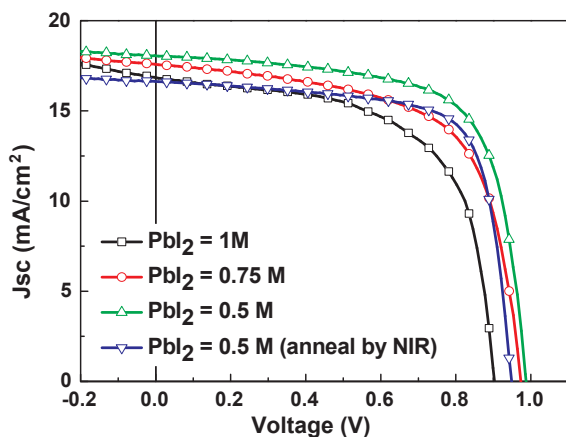


Fig. 9. J-V curves of slot-die coated perovskite solar cells by tuning the concentration of PbI_2 solution and PbI_2 anneal condition.

Table 4

Performance of slot-die coated perovskite solar cells by tuning the concentration of PbI_2 solution and PbI_2 anneal condition. Values are for the highest-PCE device, and the average data are obtained from 5 devices in the brackets.

PbI_2 Conc. (M)	J_{sc} (mA/cm^2)	V_{oc} (V)	FF (%)	PCE (%)
1	16.86 (17.31 \pm 0.32)	0.90 (0.92 \pm 0.02)	61.9 (57.9 \pm 2.9)	9.4 (9.2 \pm 0.14)
0.7	17.59 (17.73 \pm 0.17)	0.97 (0.97 \pm 0)	63.7 (61.27 \pm 2.34)	10.9 (10.53 \pm 0.33)
0.5	18.06 (18.36 \pm 0.29)	0.99 (0.98 \pm 0.01)	68.8 (66.6 \pm 1.72)	12.3 (12 \pm 0.22)
0.5 ^a	16.64 (17.18 \pm 0.56)	0.95 (0.94 \pm 0.02)	72.4 (69.77 \pm 2.02)	11.4 (11.27 \pm 0.12)

^a PbI_2 layer treated by NIR.

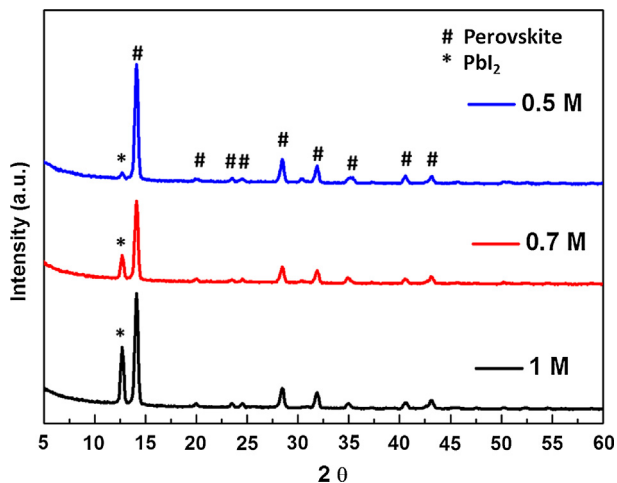


Fig. 10. XRD patterns of slot-die coated perovskite films based on various PbI_2 concentration.

remain in the perovskite films. Fig. 6(d) shows the SEM image of the NIR-NIR perovskite film in which the pin-holes increase. The reduction in PCE may be resulted from the increasing pin-holes. The synchrotron grazing-incidence wide-angle scattering and small-angle scattering (GIWAXS and GISAXS) are simultaneously performed to investigate the crystallinity, orientation and inner morphology of perovskite crystal films at the different scales (Huang et al., 2015; Liao et al., 2015; Schlipf and Müller-Buschbaum, 2017; Chang et al., 2016). Two-dimensional (2D) GIWAXS patterns of the perovskite films corresponding to the

treatments of Table 3 are shown in Fig. 5. All 2D GIWAXS patterns show the main diffraction spots corresponding to the (1 1 0) and (2 2 0) planes at scattering vector $Q = 10$ and 20 nm^{-1} , respectively, being consistent with the typical perovskite crystal structure pattern (Huang et al., 2015; Liao et al., 2015). The majority of perovskite crystallites with the (1 1 0) plane are oriented (normal) to the out-of-plane direction, as indicated by the clear diffraction spot in the Q_z direction (Huang et al., 2015). The out-of-plane direction is perpendicular to the substrate or film surface (defined as Q_z direction marked in the 2D GIWAXS pattern). The minor orientation from some perovskite crystallites is isotropic, as indicated by the diffraction rings. Their ring-averaged GIWAXS profiles are shown in Fig. 7, showing the (1 1 0), (2 2 0) and (3 3 0) peaks of perovskite structure. The similar 2D GIWAXS patterns reveal that the NIR or oven treatment cannot affect the orientation of perovskite film crystallites. The only discrepancy is that the NIR-NIR perovskite layer has an additional diffraction spot or peak at $Q = 9 \text{ nm}^{-1}$ (Figs. 6 and 7), showing the existence of PbI_2 . PbI_2 is usually produced by the decomposition of perovskite due to the insufficient thermal annealing or incomplete crystallization (Huang et al., 2015). Fig. 7 consistently shows the less intensity of perovskite peaks for the NIR-NIR annealing. The reduction in PCE for NIR-NIR perovskite can be attributed to the occurrence of decomposition to PbI_2 . On the other hand, the corresponding GISAXS profiles of these perovskite layers, as shown in Fig. 8, reveal that the inner morphology is a fractal pore network structure formed from the aggregation of primary pores with the radii of few nm, as described in our previous study (Huang et al., 2015). The shoulder of GISAXS profile of the NIR-NIR perovskite layer remarkably shifts toward the high Q region compared to the other profiles, suggesting the smaller primary pores. It is speculated that the small pores between crystallite grain boundaries may be consistently related to the incomplete crystallization. Based on the structural characterization, the fast NIR annealing instead of thermal annealing can be improved by the means of optimum of NIR irradiation.

Moreover, we also scaled up the fabrication of the perovskite solar cells by sheet-to-sheet (S2S) slot-die coating process. Different from spin-coating process, the substrate can be heated at a fixed temperature with the basic equipment during large-area S2S slot-die coating. According to above results, we slot-die coated the PbI_2 layer at a heated substrate of 70°C . The slot-die coated devices exhibits a PCE of 9.4% with a J_{sc} of $16.86 \text{ mA}/\text{cm}^2$, a V_{oc} of 0.9 V and a FF of 51.8%. The J-V curves and performance of slot-die coated perovskite solar cells are shown in Fig. 9 and listed in Table 4, respectively. As compared with the spin-coating devices, the low PCE of slot-die coated devices is mainly resulted from the reduced J_{sc} and FF. We proposed the reason is that the slot-die coated PbI_2 film is too thick to have entire perovskite phase transformation due to the characteristic of slot-die coating (all solution are retained on the substrate). Therefore, we tune the concentration of PbI_2 solution for the slot-die coated devices. The corresponding J-V curves and performances are shown in Fig. 9 and listed in Table 4, respectively. The PCE of the slot-die coated devices increases as the PbI_2 concentration decreases. The J_{sc} , V_{oc} and FF gradually increase with reducing PbI_2 concentration. This result implies that the thickness of slot-die coated PbI_2 layer can be tuned by the concentration of PbI_2 solution. The suitable thickness of PbI_2 layer is critical for the charge transport in the slot-die coated perovskite solar cells and good quality of perovskite formation. As the concentration of PbI_2 solution is 0.5 M, the highest PCE of 12.3% can be achieved. The related SEM, UV-Vis and IPCE measurements of the slot-die coated devices are shown in supporting information (Figs. S2–S4). Furthermore, we measured the film thickness of the slot-die coated PbI_2 films. The film thicknesses of PbI_2 films prepared with 1 M, 0.7 M and 0.5 M are 310 nm, 220 nm and 170 nm, respectively. In addition, the crystallinity phase of the perovskite films based on various PbI_2 films characterized by XRD is shown in Fig. 10. The residue of PbI_2 phase would be increased due to the thick PbI_2 film, and the impurity would reduce the PCE of the perovskite solar cells. This result provides a powerful evidence for the incomplete

perovskite phase formation. In addition, the negligible hysteresis behavior of the slot-die coated devices was shown in supporting information (Fig. S5). Moreover, we also apply the NIR treatment to replace the thermal treatment by oven. The performance of NIR-treated slot-die-coated devices achieves 11.4%. In addition, the related J-V curve and performance of the large-area devices with device area of 1 cm² is shown in supporting information (Fig. S6). We successfully developed the scale-up fabrication of perovskite solar cells by slot-die coating under ambient air in a short time.

4. Conclusions

We have demonstrated that it is possible to manufacture perovskite solar cells with the high efficiency over 12% in ambient condition. In addition, we also show the NIR annealing process can be used for the rapid fabrication of perovskite solar cells as compared to the traditional method widely used in literature. Further optimization of NIR annealing parameters could certainly improve the PCE of the perovskite solar cell and lead to the possibility of rapidly processed and realize the commercialization of perovskite solar cells.

Acknowledgment

The authors would like to thank the financial support from the Ministry of Science and Technology of Taiwan (Gran No. 107-2218-E-131-007).

Appendix A. Supplementary material

Supplementary data to this article can be found online at <https://doi.org/10.1016/j.solener.2018.11.020>.

References

- Chang, C.-Y., Huang, Y.-C., Tsao, C.-S., Su, W.-F., Appl, A.C.S., 2016. *Mater. Interfaces* 8, 26712–26721.
- Ciro, J., Mejía-Escobar, M.A., Jaramillo, F., 2017. *Sol. Energy* 150, 570–576.
- Cotella, G., Baker, J., Worsley, D., De Rossi, F., Pleydell-Pearce, C., Carnie, M., Watson, T., 2017. *Sol. Energy Mater. Sol. Cells* 159, 362–369.
- Das, S., Yang, B., Gu, G., Joshi, P.C., Ivanov, I.N., Rouleau, C.M., Aytug, T., Geohegan, D.B., Xiao, K., 2015. *ACS Photon.* 2, 680–686.
- De Wolf, S., Holovsky, J., Moon, S.-J., Löper, P., Niesen, B., Ledinsky, M., Haug, F.-J., Yum, J.-H., Ballif, C., 2014. *J. Phys. Chem. Lett.* 5, 1035–1039.
- Deng, Y., Peng, E., Shao, Y., Xiao, Z., Dong, Q., Huang, J., 2015. *Energy Environ. Sci.* 8, 1544–1550.
- Di Giacomo, F., Shanmugam, S., Fledderus, H., Bruijns, B.J., Verhees, W.J.H., Dorenkamper, M.S., Veenstra, S.C., Qiu, W., Gehlhaar, R., Merckx, T., Aernouts, T., Andriessen, R., Galagan, Y., 2018. *Sol. Energy Mater. Sol. Cells* 181, 53–59.
- Dualeh, A., Tétreault, N., Moehl, T., Gao, P., Nazeeruddin, M.K., Grätzel, M., 2014. *Adv. Funct. Mater.* 24, 3250–3258.
- Huang, Y.-C., Tsao, C.-S., Cho, Y.-J., Chen, K.-C., Chiang, K.-M., Hsiao, S.-Y., Chen, C.-W., Su, C.-J., Jeng, U.S., Lin, H.-W., 2015. *Sci. Rep.* 5, 13657.
- Huang, Y.-C., Cha, H.-C., Chen, C.-Y., Tsao, C.-S., 2016. *Sol. Energy Mater. Sol. Cells* 150, 10–18.
- Huang, Y.-C., Cha, H.-C., Chen, C.-Y., Tsao, C.-S., 2017. *Prog. Photovoltaics* 25, 928–935.
- Huang, H., Shi, J., Zhu, L., Li, D., Luo, Y., Meng, Q., 2016. *Nano Energy* 27, 352–358.
- Hwang, K., Jung, Y.-S., Heo, Y.-J., Scholes, F.H., Watkins, S.E., Subbiah, J., Jones, D.J., Kim, D.-Y., Vak, D., 2015. *Adv. Mater.* 27, 1241–1247.
- Jeng, J.-Y., Chiang, Y.-F., Lee, M.-H., Peng, S.-R., Guo, T.-F., Chen, P., Wen, T.-C., 2013. *Adv. Mater.* 25, 3727–3732.
- Jeon, N.J., Noh, J.H., Yang, W.S., Kim, Y.C., Ryu, S., Seo, J., Seok, S.I., 2015. *Nature* 517, 476–480.
- Kagan, C.R., Mitzi, D.B., Dimitrakopoulos, D., 1999. *Science* 286, 945–947.
- Kim, J.-E., Jung, Y.-S., Heo, Y.-J., Hwang, K., Qin, T., Kim, D.-Y., Vak, D., 2018. *Sol. Energy Mater. Sol. Cells* 179, 80–86.
- Kojima, A., Teshima, K., Shirai, Y., Miyasaka, T., 2009. *J. Am. Chem. Soc.* 131, 6050–6051.
- Liao, H.-C., Tsao, C.-S., Jao, M.-H., Hsu, C.-P., Huang, Y.-C., Tian, K.-Y., Shyue, J.-J., Chen, C.-Y., Su, C.-J., Su, W.-F., 2015. *J. Mater. Chem. A* 3, 10526–10535.
- Peiris, T.A.N., Baranwal, A.K., Kanda, H., Fukumoto, S., Kanaya, S., Cojocaru, L., Bessho, T., Miyasaka, T., Segawa, H., Ito, S., 2017. *Nanoscale* 9, 5475–5482.
- Qin, T., Huang, W., Kim, J.-E., Vak, D., Forsyth, C., McNeill, C.R., Cheng, Y.-B., 2017. *Nano Energy* 31, 210–217.
- Schlipf, J., Müller-Buschbaum, P., 2017. *Adv. Energy Mater.* 7, 1700131.
- Stranks, S.D., Eperon, G.E., Grancini, G., Menelaou, C., Alcocer, M.J., Leijtens, T., Herz, L.M., Petrozza, A., Snaith, H.J., 2013. *Science* 342, 341–344.
- Troughton, J., Charbonneau, C., Carnie, M.J., Davies, M.L., Worsley, D.A., Watson, T.M., 2015. *J. Mater. Chem. A* 3, 9123–9127.
- Troughton, J., Carnie, M.J., Davies, M.L., Charbonneau, C., Jewell, E., Worsley, D.A., Watson, T.M., 2016. *J. Mater. Chem. A* 4, 3471–3476.
- Yang, M., Li, Z., Reese, M.O., Reid, O.G., Kim, D.H., Siol, S., Klein, T.R., Yan, Y., Berry, J.J., van Hest, M.F.A.M., Zhu, K., 2017. *Nat. Energy* 2, 17038.
- Yang, W.S., Noh, J.H., Jeon, N.J., Kim, Y.C., Ryu, S., Seo, J., Seok, S.I., 2015. *Science* 348, 1234–1237.
- Yang, W.S., Park, B.-W., Jung, E.H., Jeon, N.J., Kim, Y.C., Lee, D.U., Shin, S.S., Seo, J., Kim, E.K., Noh, J.H., Seok, S.I., 2017. *Science* 356, 1376.
- Yantara, N., Sabba, D., Yanan, F., Kadro, J.M., Moehl, T., Boix, P.P., Mhaisalkar, S., Grätzel, M., Grätzel, C., 2015. *Chem. Comm.* 51, 4603–4606.
- You, J., Yang, Y., Hong, Z., Song, T.-B., Meng, L., Liu, Y., Jiang, C., Zhou, H., Chang, W.-H., Li, G., Yang, Y., 2014. *Appl. Phys. Lett.* 105, 183902.
- You, J., Hong, Z., Yang, Y., Chen, Q., Cai, M., Song, T.-B., Chen, C.-C., Lu, S., Liu, Y., Zhou, H., 2014. *ACS Nano* 8, 1674–1680.
- Yu, W., Wang, K.X., Guo, B., Qiu, X.Q., Hao, Y., Chang, J.J., Li, Y., 2017. *J. Power Sources* 358, 29–38.
- Zeng, X., Zhou, T., Leng, C., Zang, Z., Wang, M., Hu, W., Tang, X., Lu, S., Fang, L., Zhou, M., 2017. *J. Mater. Chem. A* 5, 17499–17505.
- Zhou, H., Chen, Q., Li, G., Luo, S., Song, T.B., Duan, H.S., Hong, Z., You, J., Liu, Y., Yang, Y., 2014. *Science* 345, 542–546.
- Zuo, C., Vak, D., Angmo, D., Ding, L., Gao, M., 2018. *Nano Energy* 46, 185–192.